Demirel, C., Soylu, E. (2024). Analysis of Transfer Learning-Based Algorithms for Tumor Detection in Medical Imaging Data. *The Black Sea Journal of Sciences*, 14(3), 1322-1339.

The Black Sea Journal of Sciences, 14(3), 1322-1339, 2024. DOI: 10.31466/kfbd.1455542

KFBD

Karadeniz Fen Bilimleri Dergisi
The Black Sea Journal of Sciences
ISSN (Online): 2564-7377 https://dergipark.org.tr/tr/pub/kfbd

Araştırma Makalesi / Research Article

Analysis of Transfer Learning-Based Algorithms for Tumor Detection in Medical Imaging Data

Cem DEMİREL[1], Emel SOYLU[2*]

Abstract

Magnetic Resonance Imaging (MRI) has become a vital tool in the diagnosis of brain tumors due to its non-invasive nature and high-resolution imaging capabilities. In this study, we compared the performances of deep learning algorithms. A comprehensive dataset of MRI scans was utilized to train and validate our model, ensuring robust performance across various tumor types and imaging conditions. The results demonstrate the effectiveness of our approach, achieving a high level of accuracy and sensitivity in tumor detection. Our work contributes to the development of efficient and reliable tools for early diagnosis and monitoring of brain tumors, ultimately enhancing patient care and outcomes in the field of neuroimaging. Our findings highlight the significance of selecting an appropriate deep neural network architecture when dealing with brain MRI image classification tasks. DenseNet-121 emerges as a robust choice for accurate and reliable classification, offering potential applications in clinical diagnostics and medical imaging. In conclusion, our study underscores the importance of MRI in brain tumor diagnosis and the potential of deep learning algorithms to enhance accuracy and sensitivity. Our approach, based on DenseNet-121, holds promise for clinical diagnostics and medical imaging applications, contributing to improved patient care and outcomes in neuroimaging.

Keywords: Brain tumor, MRI scans, Artificial intelligence, Computer-assisted image analyses.

MRI Verilerinde Tümör Tespiti için Transfer Tabanlı Derin Öğrenme Algoritması Karşılaştırması

Öz

Bu çalışmada, Manyetik Rezonans Görüntüleme (MRG), invazif olmayan doğası ve yüksek çözünürlüklü görüntüleme yetenekleri nedeniyle beyin tümörlerinin teşhisinde hayati bir araç haline gelmiştir. Bu çalışmada, derin öğrenme algoritmalarının performanslarını karşılaştırdık. Kapsamlı bir MRG taramaları veri kümesi, modelimizi eğitmek ve doğrulamak için kullanıldı, bu da çeşitli tümör tipleri ve görüntüleme koşulları için sağlam bir performans sağladı. Sonuçlar, yakalama konusunda yüksek bir doğruluk ve hassasiyet elde ederek yaklaşımımızın etkinliğini göstermektedir. Çalışmamız, nöro görüntüleme alanında erken teşhis ve takip için etkili ve güvenilir araçların geliştirilmesine katkıda bulunmaktadır. Bulgularımız, beyin MRG görüntü sınıflandırma görevleriyle uğraşırken uygun bir derin sinir ağı mimarisi seçmenin önemini vurgular. DenseNet-121, doğru ve güvenilir sınıflandırma için sağlam bir seçenek olarak ortaya çıkıyor ve klinik teşhis ve tıbbi görüntüleme alanlarında potansiyel uygulamalar sunuyor. Sonuç olarak, çalışmamız, MRG'nin beyin tümörü teşhisi açısından önemini ve derin öğrenme algoritmalarının doğruluğu ve hassasiyeti artırmadaki potansiyelini vurgular. DenseNet-121'e dayalı yaklaşımımız, nöro görüntüleme alanında hastaların bakımını ve sonuçlarını iyileştirmeye katkıda bulunarak klinik teşhis ve tıbbi görüntüleme uygulamaları için umut vaat etmektedir.

Anahtar Kelimeler: Beyin tümörü, MRI taramaları, Yapay zeka, Bilgisayar destekli görüntü analizleri

[1]Samsun University Department of Neurosurgery Surgical Sciences, Faculty of Medicine, Samsun, Turkey, cem.demirel@samsun.edu.tr
[2*]Samsun University, Department of Software Engineering, Faculty of Engineering, Samsun, Turkey, emel.soylu@samsun.edu.tr

[*]Sorumlu Yazar/Corresponding Author
Geliş/Received: 19.03.2024 **Kabul/Accepted:** 11.09.2024 **Yayın/Published:** 15.09.2024

1. Introduction

A brain tumor is an abnormal growth or mass of cells in the brain. It can be benign (non-cancerous) or malignant (cancerous). Brain tumors can originate from brain tissue itself (primary brain tumors) or can be the result of cancer that has spread from other parts of the body (secondary or metastatic brain tumors) (DeAngelis, 2001). Primary brain tumors are further classified based on the type of cells involved and their location within the brain. Some common types of primary brain tumors include gliomas, meningiomas, pituitary adenomas, and medulloblastomas, among others (Ayadi et al., 2021; Chandana et al., 2008; Raza et al., 2022).

According to the latest data from the World Health Organization, brain tumors are one of the most common types of cancer deaths worldwide and can occur at any age (Abd El Kader et al., 2021). Central nervous system (CNS) tumors consist of a wide series of neoplasms that include primary and metastatic tumors. While these tumors constitute approximately 1-2% of all malignancies in cancer patients, primary CNS tumors constitute 85-90% of all brain tumors (Komori, 2017; Nibhoria et al., 2015; Ostrom et al., 2015). Although they are quite rare, they have high morbidity and mortality rates. Especially in high-grade tumors such as anaplastic astrocytoma and glioblastoma, the five-year survival rate varies between 5.5–29.7% (Hernández-Hernández et al., 2018). Histopathological classification and grading of CNS tumors are very important in determining the clinical follow-up and treatment protocols of the cases and obtaining prognostic and predictive data (Cano-Valdez & Sevilla-Lizcano, 2021).

Brain tumors can cause a wide range of symptoms, depending on their size, location, and whether they are benign or malignant. Common symptoms can include headaches, seizures, changes in vision, balance problems, cognitive changes, and more (Alentorn et al., 2016).

The prognosis and treatment options for a brain tumor depend on its type, location, size, and the overall health of the patient. Treatment plans are typically developed by a multidisciplinary medical team, which may include neurosurgeons, oncologists, radiation therapists, and other specialists, to remove or control the tumor while preserving brain function and quality of life (Herholz et al., 2012). There are many more types of brain tumors, each with its unique characteristics, treatment approaches, and prognosis. The specific type of brain tumor a person has is determined through diagnostic tests such as imaging scans and biopsies, and treatment options depend on the tumor's type, location, and other factors (Sheline, 1977).

Gliomas tumors originate in the glial cells, which provide support and protection for nerve cells in the brain. Gliomas can be further categorized into astrocytomas, oligodendrogliomas, and ependymomas. Meningiomas develop in the meninges, which are the membranes covering the brain and spinal cord. They are typically benign but can cause symptoms depending on their location

(Black, 1991). Pituitary adenoma tumors form in the pituitary gland, which is a small gland at the base of the brain that regulates various hormones in the body (Theodros et al., 2015). Medulloblastomas are primarily found in the cerebellum, medulloblastomas are more common in children and are considered malignant (Baliga et al., 2021). Schwannomas tumors develop from Schwann cells, which produce the protective covering (myelin) for nerve fibers. Schwannomas can occur on nerves in the brain and spinal cord (Hilton & Hanemann, 2014). Craniopharyngiomas tumors are typically benign and develop near the pituitary gland and the hypothalamus (Momin et al., 2021). Primary Central Nervous System (CNS) Lymphomas are non-Hodgkin lymphomas that start in the brain, spinal cord, or the membranes covering the brain (Bühring et al., 2001). Metastatic Brain Tumors originate in other parts of the body and spread to the brain (Hayashida et al., 2006). Hemangioblastomas are rare tumors that usually occur in the cerebellum and are associated with a genetic condition called von Hippel-Lindau disease (Neumann et al., 1989).

Brain tumor diagnosis involves several methods and techniques to determine the presence, type, location, and characteristics of the tumor. A thorough neurological examination is often the first step. It assesses the patient's mental status, coordination, reflexes, sensory perception, and muscle strength (Pawełczyk et al., 2012). Gathering the patient's medical history, including symptoms, their duration, and any risk factors or family history of brain tumors, is crucial. MRI scans provide detailed images of the brain and can help identify the location, size, and characteristics of a brain tumor (Siddiqui et al., 2015). CT (Computed Tomography) scans use X-rays to create cross-sectional images of the brain and are useful for detecting tumors and assessing their density (Bilal, 2023). A biopsy involves the removal of a small sample of tumor tissue for examination under a microscope. This helps determine whether the tumor is benign or malignant and its specific type. If a tumor is suspected to affect the brain's ventricles or meninges, a sample of cerebrospinal fluid may be collected through a lumbar puncture (spinal tap) and analyzed for tumor markers or abnormal cells (Shankar et al., 2017). Angiography test uses a contrast dye and X-rays to visualize the blood vessels in the brain. It can help identify abnormal blood vessels or blood flow patterns associated with certain brain tumors (Taylor et al., 2014). In cases where surgery is considered, functional MRI (fMRI) or other mapping techniques can help identify critical brain regions responsible for functions such as speech or motor control to minimize damage during surgery (Gore & others, 2003). Positron Emission Tomography (PET) scans can be used to determine the metabolic activity of brain tissue, which can help differentiate between tumor tissue and healthy brain tissue (Phelps & Mazziotta, 1985). Genetic analysis may be performed to identify specific genetic mutations or markers associated with certain types of brain tumors, which can inform treatment decisions (Dulac & Wagner, 2006). Electroencephalogram (EEG) records the brain's electrical activity and may be used to evaluate seizures or abnormal brain patterns caused by tumors (Thakor & Tong, 2004). The study by Joshi and

Aziz presents a novel approach to brain tumor classification by combining Particle Swarm Optimization and Cuckoo Search with deep learning, demonstrating improved accuracy and offering valuable contributions to AI-driven tumor diagnosis and patient care (Joshi & Aziz, 2024). Kaplan et al. introduced an innovative approach for brain tumor classification using nLBP and αLBP feature extraction methods, achieving a notable classification accuracy of 95.56% with the nLBPd=1 method and K-Nearest Neighbor, contributing significantly to the automation of tumor diagnosis (Kaplan et al., 2020).

The combination of these diagnostic methods allows healthcare professionals to accurately diagnose brain tumors, determine their characteristics, and develop a tailored treatment plan for patients. The choice of diagnostic tests depends on the patient's clinical presentation and the suspected type of brain tumor.

MRI is a valuable medical imaging technique that provides detailed images of the internal structures of the body, including the brain, muscles, and organs (Katti et al., 2011). Machine learning plays a crucial role in MRI image processing for various reasons. Machine learning algorithms can enhance the quality of MRI images by reducing noise, improving contrast, and sharpening details. This results in clearer and more diagnostically valuable images. ML techniques can accelerate MRI image reconstruction, reducing the time patients spend in the scanner. Faster reconstruction is particularly important for pediatric and critically ill patients. ML models can segment MRI images into different regions or structures, such as tumors, organs, or blood vessels. This automated process saves time for radiologists and ensures accuracy in identifying specific areas of interest. Machine learning can aid in the detection of abnormalities or diseases in MRI images, such as tumors, lesions, or vascular issues. ML models can learn to recognize subtle patterns that might be missed by human observers. ML algorithms can provide quantitative measurements of various parameters in MRI images, such as tumor size, tissue density, or blood flow. This quantitative data is crucial for treatment planning and monitoring disease progression. ML can analyze historical MRI data and patient records to predict disease outcomes, treatment responses, or the likelihood of disease recurrence. This information can guide treatment decisions and improve patient care. Machine learning is essential in MRI image processing because it enhances image quality, automates time-consuming tasks, assists in disease detection, and contributes to research and innovation in medical imaging. These applications ultimately lead to more accurate diagnoses, better patient care, and advancements in the field of radiology (Ayadi et al., 2021; Deepak & Ameer, 2019).

Brain tumor detection relies on various computer algorithms and image processing techniques to analyze and interpret medical images, particularly MRI and CT scans. Deep learning techniques have ushered in a remarkable era of progress in the realm of brain tumor diagnosis. These sophisticated algorithms, particularly Convolutional Neural Networks (CNNs), have exhibited an

extraordinary capacity to decipher intricate patterns within medical images, especially MRI and CT scans. Their ability to automatically extract and learn hierarchical features from vast datasets has led to unparalleled accuracy in identifying and characterizing brain tumors. Deep learning's prowess extends beyond mere detection; it enables precise segmentation, tumor volume estimation, and even prediction of treatment response. The amalgamation of deep learning's prowess with medical imaging has revolutionized the field, offering not only enhanced diagnostic capabilities but also the potential to improve patient outcomes by facilitating early detection and personalized treatment strategies. As these algorithms continue to evolve, the future of brain tumor diagnosis holds immense promise, with deep learning at its forefront, exemplifying the synergy between artificial intelligence and healthcare (Ayadi et al., 2021; Chattopadhyay & Maitra, 2022; Deepak & Ameer, 2019; Senan et al., 2022). Mahalty et al. present a novel deep learning model for MRI-based brain tumor classification that integrates a soft attention mechanism and multi-layer feature aggregation, demonstrating superior performance compared to state-of-the-art models in enhancing classification accuracy.

In this study, we present a comprehensive comparative analysis of various deep neural network architectures for the classification of brain MRI images. The primary objective of this research is twofold: first, to classify images into two categories, "Tumor" and "No Tumor," and second, to further classify tumor images into four specific subcategories: "Glioma," "Meningioma," "No Tumor," and "Pituitary." Our evaluation focuses on the following deep learning architectures: DenseNet-121, DenseNet-201, Xception, EfficientNetV2B3, EfficientNetV2S, EfficientNetB0, InceptionV3, MobileNet, and ResNet-50. Through an extensive experimentation process, we have assessed the performance of these architectures using various evaluation metrics, including accuracy, precision, recall, F1 score, and overall accuracy. Remarkably, DenseNet-121 consistently outperforms the other architectures in both binary tumor classification and multi-class tumor subtype classification tasks. Its ability to capture intricate features within the MRI images results in superior classification accuracy.

2. Relevant Work

Over the last two decades, medical image analysis has gained significant attention due to its broad healthcare applications, particularly in patient investigation and diagnosis. Various studies have explored machine learning-based approaches for brain image classification and analysis, including the comparison of traditional machine learning and deep learning methods. Additionally, some studies have introduced innovative techniques for brain tumor segmentation and localization, achieving high precision in cancer detection from MRI scans.

Table 1. Relevant work

Ref.	Dataset	Tumor Type	Method	Result
(Abiwinanda et al., 2019)	Cheng (Brain Tumor Dataset (Cheng, 2017)	Glioma, Meningioma, and Pituitary	CNN	training accuracy of 98.51% and validation accuracy of 84.19% at best
(Seetha & Raja, 2018)	tumor and nontumor MRI images collected from different online resources	Tumor, Non-tumor	SVM, DNN, CNN	training accuracy of 97.5%
(Deepak & Ameer, 2019)	Cheng (Brain Tumor Dataset (Cheng, 2017)	Glioma, Meningioma, and Pituitary	Transfer learning based on CNN	a mean classification accuracy of 98%
(Ayadi et al., 2021)	Figshare (Cheng, 2017), Radiopaedia	Glioma, Meningioma, and Pituitary	CNN	Overall accuracy between 90.35% and 99.61%
(Raza et al., 2022)	Figshare (Cheng, 2017)	Glioma, Meningioma, and Pituitary	Hybrid deep learning	99.67% accuracy
(Abdusalomov et al., 2023)	MRI scan images (*Brain Tumor Classification (MRI)*, n.d.; *Brain Tumor MRI Dataset*, n.d.)	Tumor, Non-tumor	YOLOv7	99.5% accuracy
(Afshar et al., 2019)	MRI scan images (Cheng et al., 2016)	Glioma, Meningioma, and Pituitary	Capsule Network	90.8% accuracy

Despite substantial progress in this field, there is still a need for novel methodologies to enhance feature extraction, tumor classification, and localization efficacy. These studies collectively emphasize the significant potential of deep learning in improving brain tumor diagnosis and analysis from medical images. Table 1 This table provides information about various references, datasets, tumor types, methods used, and the corresponding results in different studies related to brain tumor detection and classification.

3. Dataset

We utilized a publicly accessible MRI dataset acquired from Kaggle.com (*Brain Tumor Classification (MRI)*, n.d.; Cheng et al., 2016). There are 926 instances of the 'Glioma' class, 937 instances of the 'Meningioma' class, 901 instances of the 'Pituitary' class, and 500 instances categorized as 'Non-tumor.'

The initial dataset preparation step involves cropping the brain from the images. We used Adrian Rosebrock's source code for this progress (*Finding Extreme Points in Contours with OpenCV*, n.d.). Class-wise sample images from the dataset are given in Figure 1.

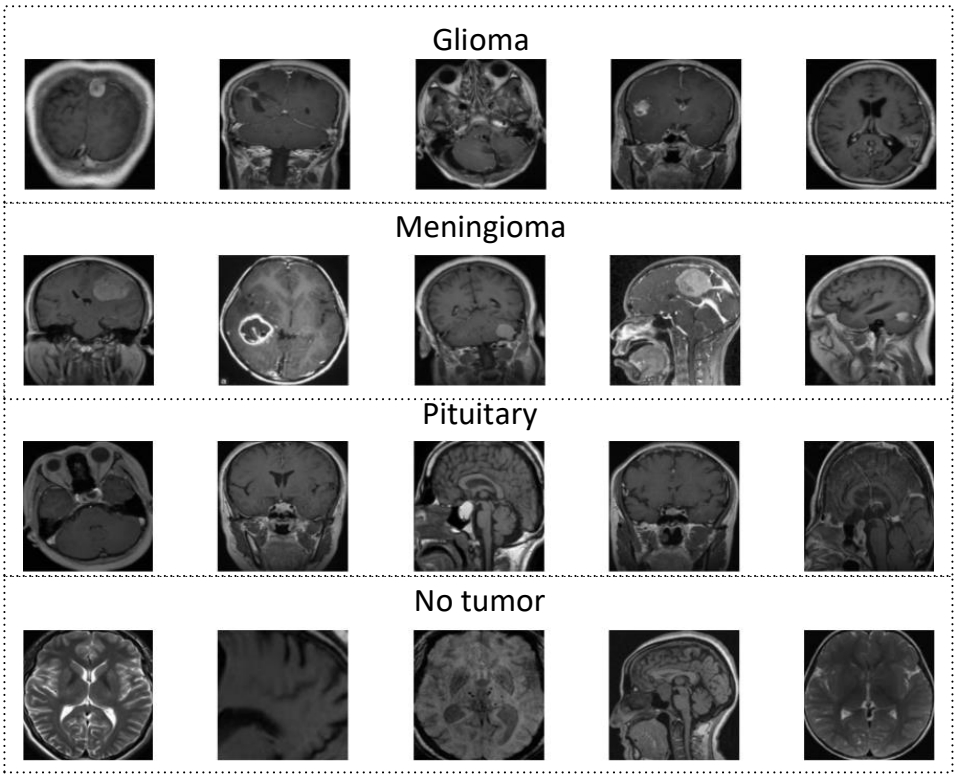

Figure 1. Class-wise sample images from the dataset

We utilized this dataset in two ways. In the first approach, we classified the brain images into two categories: tumor and no tumor. In the second approach, we classified them into four categories: Glioma, Meningioma, Pituitary, and No tumor. We split the data into training, validation, and test sets.

In the first approach, the training set comprises 1,990 Tumor samples and 360 No-tumor samples, while the validation set consists of 496 Tumor samples and 90 No-tumor samples. Finally, the test set is composed of 278 Tumor samples and 50 No-tumor samples.

In the second approach, the training set contains 667 Glioma samples, 675 Meningioma samples, 648 Pituitary samples, and 360 No tumor samples. In the validation set, there are 166 Glioma samples, 168 Meningioma samples, 162 Pituitary samples, and 90 No tumor samples. Lastly, the test set includes 93 Glioma samples, 94 Meningioma samples, 91 Pituitary samples, and 50 No-tumor samples.

4. Method

We used transfer learning-based deep learning models in our study. Transfer Learning in the context of deep learning refers to the practice of leveraging a pre-trained neural network model for a new, related task. It's a technique where a model developed for a particular task is adapted for a second related task. Transfer learning can significantly speed up the training process and often leads

to better performance compared to training a model from scratch. Transfer learning typically involves starting with a pre-trained model that has been trained on a large dataset for a similar or related problem. These models are often trained on massive datasets and have learned useful features from them. After obtaining a pre-trained model, you fine-tune it for your specific task. Training deep neural networks from scratch can be computationally expensive and time-consuming, especially when dealing with large datasets and complex architectures. Transfer learning allows you to start with a pre-trained model, saving a significant amount of training time.

We have leveraged a selection of pre-trained CNN architectures, including DenseNet121, DenseNet201, Xception, EfficientNetV2B3, EfficientNetV2S, EfficientNetB0, InceptionV3, MobileNet, and ResNet-50, for brain tumor classification. These models can be readily accessed in Keras, an open-source neural network library written in Python (*Keras Applications*, n.d.).

DenseNet, short for "Densely Connected Convolutional Network," is a deep learning architecture for image classification and computer vision tasks. It was introduced by Gao Huang, Zhuang Liu, and Laurens van der Maaten in their 2017 paper titled "Densely Connected Convolutional Networks." DenseNet builds on the concept of skip connections, also known as residual connections, used in ResNet architectures. In a DenseNet, each layer is connected not only to the layers immediately before and after it but also to all the previous layers in a dense and highly interconnected manner. This dense connectivity pattern enables feature reuse, reduces the number of parameters, and mitigates the vanishing gradient problem during training (Huang et al., 2017). DenseNet architectures come in various versions, including DenseNet-121, DenseNet-169, DenseNet-201, and others, each with a different number of layers. DenseNet has achieved state-of-the-art results on various image classification tasks and is widely used in computer vision applications due to its efficiency and effectiveness in training deep neural networks.

Inception, also known as GoogleNet, is a deep learning architecture for convolutional neural networks (CNNs) that was designed to address the challenges of training very deep networks while managing computational efficiency. Introduced by Google researchers, Inception employs a unique and innovative "Inception module" that incorporates multiple convolutional filter sizes and pooling operations within a single layer. This enables the network to capture features at various scales, facilitating more robust and accurate feature extraction. Inception has been influential in the field of computer vision, particularly in image classification and object detection tasks, and its ability to balance model depth with computational efficiency has made it a widely used architecture in deep learning (Szegedy et al., 2016).

EfficientNet is a family of deep learning models specifically designed to achieve state-of-the-art performance with high efficiency in terms of computational resources. These models use a novel scaling method that uniformly scales the network's depth, width, and resolution. This approach

ensures that the model adapts to different computational constraints while maintaining excellent performance on a wide range of computer vision tasks, such as image classification and object detection. EfficientNet's architecture efficiently balances model size and accuracy, making it a popular choice for various real-world applications where computational efficiency is a priority, such as edge devices and resource-constrained environments (Tan & Le, 2019).

Xception, short for "Extreme Inception," is a deep learning model designed for computer vision tasks, particularly image classification and object detection. Developed by Google researchers, Xception is based on the Inception architecture and focuses on enhancing feature extraction through depthwise separable convolutions, which separate the convolution process into two stages: depthwise and pointwise convolutions. This separation of operations aims to capture complex patterns more effectively and efficiently, making the model more robust while reducing the number of parameters. Xception has proven to be highly effective in various visual recognition tasks, offering excellent accuracy and performance in deep learning applications (Chollet, 2017).

ResNet, or Residual Neural Network, is a deep learning architecture that revolutionized the field of computer vision. It was introduced by Kaiming He et al. in 2016. What sets ResNet apart from previous architectures is its use of residual blocks, which allow for the training of very deep neural networks without the vanishing gradient problem. In a residual block, the input to a layer is combined with the output of the layer, allowing the network to learn residual functions. This approach enables the training of extremely deep networks, with hundreds or even thousands of layers, leading to improved accuracy in tasks like image classification and object detection. ResNet's architecture has become a fundamental building block for many state-of-the-art neural network architectures in various domains beyond computer vision (He et al., 2016).

The general block diagram of the system is given in Figure 2. In the preprocessing stage, the dataset has been divided into training, validation, and test data sets after the data splitting process. Parameters have been configured for the preferred models for transfer learning. For all architectures, a batch size of 32 and an epoch count of 40 have been determined. This choice was made through trial and error, and it was deemed sufficient to achieve the best results after 40 epochs. In the second stage, pre-trained architectures were retrained using the training data. Prediction accuracy rates were obtained using both the training data and the validation data. In the third stage, completed training architectures were evaluated using the test data as input, and evaluation results were obtained based on performance metrics. Performance metrics utilized the True Positive, True Negative, False Negative (FN), and False Positive (FP) values obtained from the classification results on the test data.

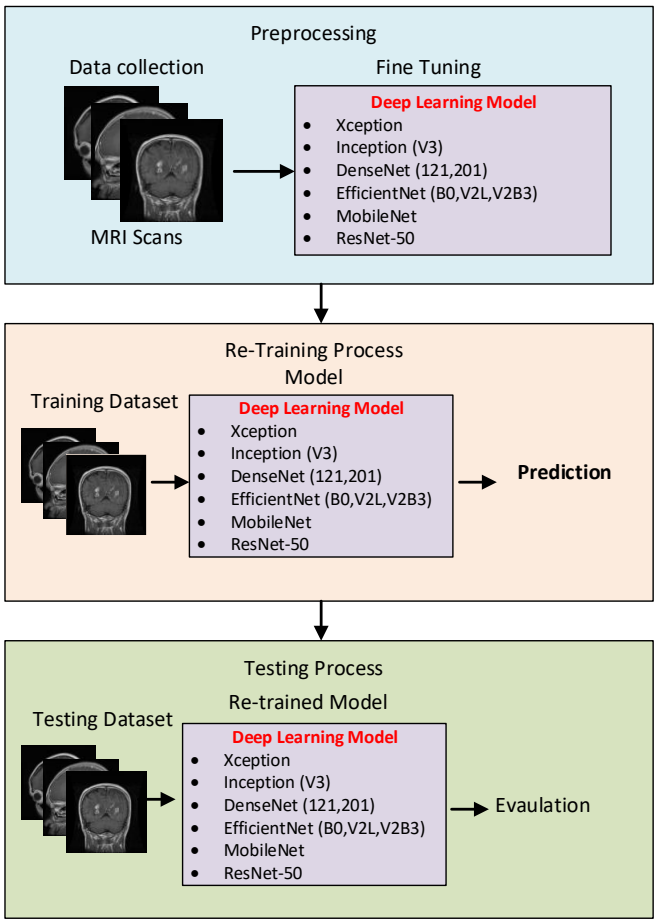

Figure 2. Block diagram of the system

In the context of classification True Positive (TP) refers to the number of cases correctly predicted as positive when they are actually positive. True Negative (TN) refers to the number of cases correctly predicted as negative when they are actually negative. False Negative (FN), also known as a type two error, represents the number of cases incorrectly predicted as negative when they are actually positive. False Positive (FP), also known as a type one error, denotes the number of cases incorrectly predicted as positive when they are actually negative.

Precision, recall, F1 score, and accuracy are performance metrics that help evaluate the performance of a classification model. Eq.1-4 are the formulas for these metrics. Precision (P) measures the accuracy of positive predictions made by the model (Raschka, 2014) as given in Eq. 1.

$$P = \frac{TP}{TP+FP} \tag{1}$$

Recall, also known as True Positive Rate or Sensitivity, measures the ability of the model to identify all positive instances correctly. The equation of recall is given in Eq. 2.

$$R = \frac{TP}{TP+FN} \quad (2)$$

The F1 Score is the harmonic mean of precision and recall. It provides a balance between precision and recall and is particularly useful when dealing with imbalanced datasets. The equation of F1 is given in Eq.3.

$$F1\ Score = 2 \cdot \frac{P \cdot R}{P+R} \quad (3)$$

Accuracy measures the overall correctness of predictions made by the model. The equation of accuracy is given in Eq. 4.

$$Accuracy = \frac{TP+TN}{TP+TN+FP+FN} \quad (4)$$

5. Results

For the first approach, DenseNet-121 provided the highest accuracy rate on the validation data. In Table 2, we present the training performance metrics for nine different base models used in the first approach. The table provides an overview of the training and validation performance of these base models, including their training accuracy, accuracy loss, validation accuracy, and validation loss. The models with the highest training accuracy are MobileNet, DenseNet-121, and DenseNet-201 achieving a perfect training accuracy of 100%. This indicates that MobileNet, DenseNet-121, and DenseNet-201 have successfully learned and adapted to the training data, fitting it very closely. On the other hand, the model with the highest validation accuracy is DenseNet-121, with a validation accuracy of 98.81%. This suggests that DenseNet-121 performed exceptionally well on data it hasn't seen during training, demonstrating its robustness and effectiveness in generalizing to new, unseen examples. These results indicate that MobileNet excels in fitting the training data closely, while DenseNet-121 is particularly adept at achieving high accuracy on new, previously unseen data during validation.

Table 2. Training performance table for first approach

Base Model	Training Accuracy	Acc-loss	Validation accuracy	Val-loss
DenseNet-121	100%	6.62E-01	98.81%	0.1437
Densenet-201	100%	1.37E+00	98.64%	0.0605
Xception	99.96%	0.0017	97.31%	0.0653
EfficientNetV2B3	99.49%	0.0142	97.27%	0.0701
EfficientNetV2S	99.62%	0.0095	97.27%	0.1571
EfficientNetB0	99.96%	0.002	98.13%	0.0794
InceptionV3	99.74%	0.005	96.76%	0.1517
MobileNet	100%	7.60E-02	97.61%	0.0918
Resnet-50	99.11%	0.0275	96.76%	0.1393

Figure 3 displays the confusion matrices obtained from the test data inputs for the nine re-trained architectures. The performance metrics for re-trained models in the first approach can be found in Table 3. In this context, "n truth" represents the number of actual cases within a class, while "n classified" indicates the count of cases classified as belonging to that class. These performance metrics are derived from the confusion matrices presented in Figure 3.

Table 3. Performance metrics of re-trained models for the first approach

Method	Class	n truth	n classified	Precision	Recall	F1 Score	Overall Accuracy
MobileNet	No Tumor	67	50	0.96	0.72	0.82	93.56%
	Tumor	259	276	0.93	0.99	0.99	
DenseNet-121	No Tumor	64	50	0.98	0.77	0.86	**95.09%**
	Tumor	262	276	0.95	1.0	0.97	
DenseNet-201	No Tumor	66	50	0.96	0.73	0.73	93.87%
	Tumor	260	276	0.93	0.99	0.99	
Xception	No Tumor	59	50	0.92	0.78	0.84	94.79%
	Tumor	267	276	0.95	0.99	0.97	
Inception-V3	No Tumor	61	50	0.92	0.75	0.83	94.17%
	Tumor	265	276	0.95	0.98	0.96	
EfficientNet-B0	No Tumor	70	50	0.98	0.70	0.82	93.25%
	Tumor	256	276	0.92	1.0	0.96	
EfficientNet-V2B3	No Tumor	68	50	0.98	0.72	0.83	93.87%
	Tumor	258	276	0.93	1.0	0.96	
EfficientNet-V2S	No Tumor	64	50	0.92	0.72	0.81	93.25%
	Tumor	262	276	0.93	0.98	0.96	
ResNet-50	No Tumor	60	50	0.82	0.68	0.75	91.41%
	Tumor	256	276	0.93	0.97	0.95	

Among the models, both MobileNet and DenseNet-201 achieved the highest F1 score for the "Tumor" class, while ResNet-50 recorded the lowest F1 score for this class. For the "No Tumor" class, DenseNet-121 secured the highest F1 score, while ResNet-50 again had the lowest F1 score. Notably, DenseNet-121 emerged as the model with the highest overall accuracy, showcasing its exceptional proficiency in correctly classifying "Tumor" cases with precision, recall, and overall

accuracy. Conversely, ResNet-50 exhibited the lowest overall accuracy among all models, particularly when classifying both "No Tumor" and "Tumor" cases, indicating a relatively higher rate of misclassifications in comparison to the other models.

Model	MobileNet			Model	DenseNet-121			Model	DenseNet-201		
P/T	Predicted			P/T	Predicted			P/T	Predicted		
True	Class	No Tumor	Tumor	True	Class	No Tumor	Tumor	True	Class	No Tumor	Tumor
	No Tumor	48	2		No Tumor	49	1		No Tumor	48	2
	Tumor	19	257		Tumor	15	261		Tumor	18	258
Model	Xception			Model	Inception-V3			Model	EfficientNet-B0		
P/T	Predicted			P/T	Predicted			P/T	Predicted		
True	Class	No Tumor	Tumor	True	Class	No Tumor	Tumor	True	Class	No Tumor	Tumor
	No Tumor	46	4		No Tumor	46	4		No Tumor	49	1
	Tumor	13	263		Tumor	15	261		Tumor	21	255
Model	EfficientNet-V2B3			Model	EfficientNet-V2S			Model	ResNet-50		
P/T	Predicted			P/T	Predicted			P/T	Predicted		
True	Class	No Tumor	Tumor	True	Class	No Tumor	Tumor	True	Class	No Tumor	Tumor
	No Tumor	49	1		No Tumor	46	4		No Tumor	41	9
	Tumor	19	257		Tumor	18	258		Tumor	19	257

Figure 3. Confusion matrixes for the first approach

DenseNet-121 architecture provided the highest accuracy rate on the validation data for the second approach. Table 4 provides an overview of the training and validation performance of nine base models for the second approach. It includes their training accuracy, accuracy loss, validation accuracy, and validation loss. These metrics help assess how well each model has been trained and how it generalizes to new data. The table provides an overview of the training and validation performance of these base models. It includes their training accuracy, accuracy loss, validation accuracy, and validation loss. These metrics help assess how well each model has been trained and how it generalizes to new data.

Table 4. Training performance table for first approach

Base Model	Training Accuracy	Acc-loss	Validation accuracy	Val-loss
DenseNet121	99.49	0.0162	84.48	0.7303
Densenet201	99.06	0.0231	69.45	23.455
Xception	99.78	0.0081	89.93	0,5774
EfficientNetV2B3	99.15	0.0309	90.61	0.3279
EfficientNetV2S	99.49	0.0181	91.98	0.2974
EfficientNetB0	98.89	0.0362	73.04	12.469
InceptionV3	98.98	0.0272	78.67	14.649
MobileNet	99.66	0.0119	88.4	0.6248
Resnet-50	99.4	0.0248	85.15	0.7683

Figure 4 displays the confusion matrices obtained from the test data inputs for the nine re-trained architectures.

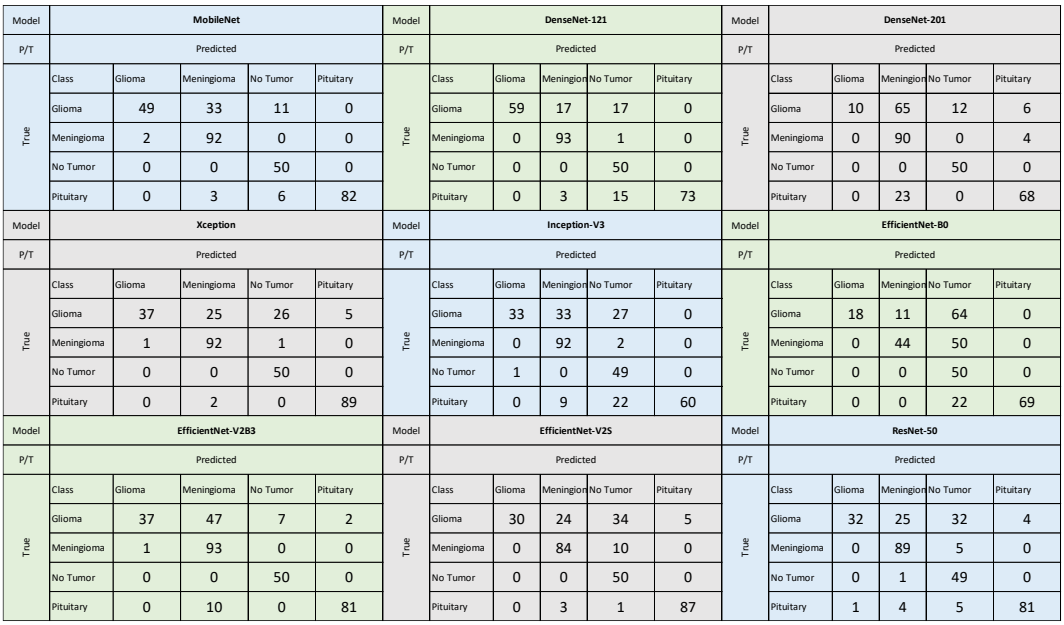

Model	MobileNet					Model	DenseNet-121					Model	DenseNet-201				
P/T	Predicted					P/T	Predicted					P/T	Predicted				
True	Class	Glioma	Meningioma	No Tumor	Pituitary	True	Class	Glioma	Meningiom	No Tumor	Pituitary	True	Class	Glioma	Meningiom	No Tumor	Pituitary
	Glioma	49	33	11	0		Glioma	59	17	17	0		Glioma	10	65	12	6
	Meningioma	2	92	0	0		Meningioma	0	93	1	0		Meningioma	0	90	0	4
	No Tumor	0	0	50	0		No Tumor	0	0	50	0		No Tumor	0	0	50	0
	Pituitary	0	3	6	82		Pituitary	0	3	15	73		Pituitary	0	23	0	68
Model	Xception					Model	Inception-V3					Model	EfficientNet-B0				
P/T	Predicted					P/T	Predicted					P/T	Predicted				
True	Class	Glioma	Meningioma	No Tumor	Pituitary	True	Class	Glioma	Meningiom	No Tumor	Pituitary	True	Class	Glioma	Meningiom	No Tumor	Pituitary
	Glioma	37	25	26	5		Glioma	33	33	27	0		Glioma	18	11	64	0
	Meningioma	1	92	1	0		Meningioma	0	92	2	0		Meningioma	0	44	50	0
	No Tumor	0	0	50	0		No Tumor	1	0	49	0		No Tumor	0	0	50	0
	Pituitary	0	2	0	89		Pituitary	0	9	22	60		Pituitary	0	0	22	69
Model	EfficientNet-V2B3					Model	EfficientNet-V2S					Model	ResNet-50				
P/T	Predicted					P/T	Predicted					P/T	Predicted				
True	Class	Glioma	Meningioma	No Tumor	Pituitary	True	Class	Glioma	Meningiom	No Tumor	Pituitary	True	Class	Glioma	Meningiom	No Tumor	Pituitary
	Glioma	37	47	7	2		Glioma	30	24	34	5		Glioma	32	25	32	4
	Meningioma	1	93	0	0		Meningioma	0	84	10	0		Meningioma	0	89	5	0
	No Tumor	0	0	50	0		No Tumor	0	0	50	0		No Tumor	0	1	49	0
	Pituitary	0	10	0	81		Pituitary	0	3	1	87		Pituitary	1	4	5	81

Figure 4. Confusion matrixes for the second approach

The performance metrics for re-trained models in the second approach are provided in Table 5. These metrics were computed based on the confusion matrices presented in Figure 4. In the Glioma class, DenseNet-121 achieved the highest F1 Score and Overall Accuracy, while DenseNet-201 recorded the lowest F1 score. For the Meningioma class, DenseNet-201 attained the highest F1 Score, while EfficientNet-V2B3 had the lowest F1 score. In the No Tumor class, EfficientNet-V2B3 secured the highest F1 Score, while EfficientNet-B0 had the lowest F1 score. Regarding the Pituitary class, Xception demonstrated the highest F1 Score, while Inception-V3 exhibited the lowest F1 score. Notably, the DenseNet-121 model achieved the best overall accuracy, whereas the EfficientNet-B0 model recorded the lowest overall accuracy among all models.

Table 5. Performance metrics of re-trained models for the second approach

Method	Class	n truth	n classified	Acc.	Precision	Recall	F1 Score	Overall Acc.
MobileNet	Glioma	51	93	85.98%	0.53	0.96	0.68	83.23%
	Meningioma	128	94	88.41%	0.98	0.72	0.83	
	No Tumor	67	50	94.82%	1.0	0.75	0.85	
	Pituitary	82	91	97.26%	0.9	1.0	0.95	
DenseNet-121	Glioma	59	93	89.63%	0.63	1.0	**0.78**	**83.84%**
	Meningioma	113	94	93.6%	0.99	0.82	0.9	
	No Tumor	83	50	89.94%	1.0	0.6	0.75	
	Pituitary	73	91	94.51%	0.8	1.0	0.89	
DenseNet-201	Glioma	10	93	74.7%	0.11	1.0	0.19	64.46%
	Meningioma	178	94	71.95%	0.96	0.51	**1.0**	

Xception	No Tumor	62	50	96.54%	1.0	0.81	0.89	81.71%
	Pituitary	78	91	89.94%	0.75	0.87	0.8	
	Glioma	38	93	82.62%	0.4	0.97	0.56	
	Meningioma	119	94	91.16%	0.98	0.77	0.86	
	No Tumor	77	50	91.77%	1.0	0.65	0.79	
	Pituitary	94	91	97.87%	0.98	0.95	**0.96**	
Inception-V3	Glioma	34	93	81.4%	0.35	0.97	0.52	71.34%
	Meningioma	134	94	86.59%	0.98	0.69	0.81	
	No Tumor	100	50	84.15%	0.98	0.49	0.65	
	Pituitary	60	91	90.55%	0.66	1.0	0.79	
EfficientNet-B0	Glioma	18	93	77.13%	0.19	1.0	0.32	55.18%
	Meningioma	55	94	81.4%	0.47	0.8	0.59	
	No Tumor	186	50	58.54%	1.0	0.27	0.42	
	Pituitary	69	91	93.29%	0.76	1.0	0.86	
EfficientNet-V2B3	Glioma	38	93	82.62%	0.4	0.97	0.56	79.57%
	Meningioma	150	94	82.32%	0.99	0.62	0.76	
	No Tumor	57	50	97.87%	1.0	0.88	**0.93**	
	Pituitary	83	91	96.34%	0.89	0.98	0.93	
EfficientNet-V2S	Glioma	30	93	80.79%	0.32	1.0	0.49	76.52%
	Meningioma	111	94	88.72%	0.89	0.76	0.82	
	No Tumor	95	50	86.28%	1.0	0.53	0.69	
	Pituitary	92	91	97.26%	0.96	0.99	0.95	
ResNet-50	Glioma	33	93	81.1%	0.34	0.97	0.51	76.52%
	Meningioma	119	94	89.33%	0.95	0.75	0.84	
	No Tumor	91	50	86.89%	0.98	0.54	0.7	
	Pituitary	85	91	95.73%	0.89	0.95	0.92	

6. Conclusions

In conclusion, this study harnessed the capabilities of deep learning algorithms to advance the detection and diagnosis of brain tumors through MRI scans. By utilizing a comprehensive dataset that captured a wide range of tumor types and imaging conditions, our model demonstrated robustness and adaptability. The results highlighted the efficacy of the proposed approach, achieving high accuracy and sensitivity in tumor detection. This contribution is instrumental in developing reliable tools for the early diagnosis and monitoring of brain tumors, offering significant potential for improving patient care in neuroimaging.

A key aspect of the study was the careful selection of deep neural network architectures for the brain MRI image classification task. DenseNet-121 emerged as a particularly effective model, consistently providing accurate and reliable classifications. In our binary classification approach, which categorized images as tumor and no tumor, MobileNet, DenseNet-121, and DenseNet-201 all achieved perfect training accuracy. However, DenseNet-121 excelled in generalization, with a validation accuracy of 98.81%. In the multi-class classification, which differentiated between four tumor categories, DenseNet-121 again outperformed the other models, recording the highest F1 Scores and overall accuracy, especially in the Glioma and No Tumor classes. DenseNet-201 and EfficientNet-B0, in contrast, demonstrated lower F1 Scores, underscoring the critical importance of model architecture in deep learning applications.

This study underscores the transformative potential of deep learning in medical imaging, particularly in enhancing the precision of brain tumor detection and classification. Our findings highlight the importance of model selection for achieving optimal performance in clinical diagnostics, marking a step forward in the application of AI in healthcare.

In the future, several avenues can be explored to extend the findings of this study and further enhance deep learning-based brain tumor diagnosis methods. Firstly, testing the model's performance on larger and more diverse datasets could improve its generalization ability, particularly in diagnosing rare tumor types. Additionally, the use of more complex deep learning architectures, especially hybrid models and Transformer-based approaches, can be investigated. Integrating explainable artificial intelligence (XAI) methods could support the clinical use of the model by allowing doctors to trust these tools more confidently in decision-making processes. Finally, training the model with multimodal data sources, such as combining different medical imaging modalities (CT, PET, etc.), could provide a more comprehensive perspective in brain tumor diagnosis and monitoring. Such improvements could broaden the application of deep learning in the medical field and offer more effective solutions in clinical practice.

Authors' Contributions

All authors contributed equally to the study.

Statement of Conflicts of Interest

There is no conflict of interest between the authors.

Statement of Research and Publication Ethics

The author declares that this study complies with Research and Publication Ethics.

References

Abd El Kader, I., Xu, G., Shuai, Z., Saminu, S., Javaid, I., & Salim Ahmad, I. (2021). Differential deep convolutional neural network model for brain tumor classification. *Brain Sciences, 11*(3), 352.

Abdusalomov, A. B., Mukhiddinov, M., & Whangbo, T. K. (2023). Brain Tumor Detection Based on Deep Learning Approaches and Magnetic Resonance Imaging. *Cancers, 15*(16), 4172.

Abiwinanda, N., Hanif, M., Hesaputra, S. T., Handayani, A., & Mengko, T. R. (2019). Brain tumor classification using convolutional neural network. *World Congress on Medical Physics and Biomedical Engineering 2018: June 3-8, 2018, Prague, Czech Republic (Vol. 1)*, 183–189.

Afshar, P., Plataniotis, K. N., & Mohammadi, A. (2019). Capsule networks for brain tumor classification based

on MRI images and coarse tumor boundaries. *ICASSP 2019-2019 IEEE International Conference on Acoustics, Speech and Signal Processing (ICASSP)*, 1368–1372.

Alentorn, A., Hoang-Xuan, K., & Mikkelsen, T. (2016). Presenting signs and symptoms in brain tumors. *Handbook of Clinical Neurology*, *134*, 19–26.

Ayadi, W., Elhamzi, W., Charfi, I., & Atri, M. (2021). Deep CNN for brain tumor classification. *Neural Processing Letters*, *53*, 671–700.

Baliga, S., Gandola, L., Timmermann, B., Gail, H., Padovani, L., Janssens, G. O., & Yock, T. I. (2021). Brain tumors: Medulloblastoma, ATRT, ependymoma. *Pediatric Blood \& Cancer*, *68*, e28395.

Bilal, H. (2023). *Computed Tomography (CT) Scanning: Principles and Applications*.

Black, P. M. (1991). Brain tumors. *New England Journal of Medicine*, *324*(22), 1555–1564.

Brain Tumor Classification (MRI). (n.d.). https://www.kaggle.com/datasets/sartajbhuvaji/brain-tumor-classification-mri

Brain Tumor MRI Dataset. (n.d.). https://www.kaggle.com/datasets/masoudnickparvar/brain-tumor-mri-dataset

Bühring, U., Herrlinger, U., Krings, T., Thiex, R., Weller, M., & Küker, W. (2001). MRI features of primary central nervous system lymphomas at presentation. *Neurology*, *57*(3), 393–396.

Cano-Valdez, A. M., & Sevilla-Lizcano, D. B. (2021). Pathological classification of brain tumors. *Principles of Neuro-Oncology: Brain \& Skull Base*, 75–105.

Chandana, S. R., Movva, S., Arora, M., & Singh, T. (2008). Primary brain tumors in adults. *American Family Physician*, *77*(10), 1423–1430.

Chattopadhyay, A., & Maitra, M. (2022). MRI-based brain tumour image detection using CNN based deep learning method. *Neuroscience Informatics*, *2*(4), 100060.

Cheng. (2017). *brain tumor dataset*. https://doi.org/10.6084/m9.figshare.1512427.v5

Cheng, J., Yang, W., Huang, M., Huang, W., Jiang, J., Zhou, Y., Yang, R., Zhao, J., Feng, Y., Feng, Q., & others. (2016). Retrieval of brain tumors by adaptive spatial pooling and fisher vector representation. *PloS One*, *11*(6), e0157112.

Chollet, F. (2017). Xception: Deep learning with depthwise separable convolutions. *Proceedings of the IEEE Conference on Computer Vision and Pattern Recognition*, 1251–1258.

DeAngelis, L. M. (2001). Brain tumors. *New England Journal of Medicine*, *344*(2), 114–123.

Deepak, S., & Ameer, P. M. (2019). Brain tumor classification using deep CNN features via transfer learning. *Computers in Biology and Medicine*, *111*, 103345.

Dulac, C., & Wagner, S. (2006). Genetic analysis of brain circuits underlying pheromone signaling. *Annu. Rev. Genet.*, *40*, 449–467.

Finding extreme points in contours with OpenCV. (n.d.). https://pyimagesearch.com/2016/04/11/finding-extreme-points-in-contours-with-opencv/

Gore, J. C., & others. (2003). Principles and practice of functional MRI of the human brain. *The Journal of Clinical Investigation*, *112*(1), 4–9.

Hayashida, Y., Hirai, T., Morishita, S., Kitajima, M., Murakami, R., Korogi, Y., Makino, K., Nakamura, H., Ikushima, I., Yamura, M., & others. (2006). Diffusion-weighted imaging of metastatic brain tumors: comparison with histologic type and tumor cellularity. *American Journal of Neuroradiology*, *27*(7), 1419–1425.

He, K., Zhang, X., Ren, S., & Sun, J. (2016). Deep residual learning for image recognition. *Proceedings of the IEEE Conference on Computer Vision and Pattern Recognition*, 770–778.

Herholz, K., Langen, K.-J., Schiepers, C., & Mountz, J. M. (2012). Brain tumors. *Seminars in Nuclear Medicine*, *42*(6), 356–370.

Hernández-Hernández, A., Reyes-Moreno, I., Gutiérrez-Aceves, A., Guerrero-Juárez, V., Santos-Zambrano, J., López-Mart\'\inez, M., Castro-Mart\'\inez, E., Cacho-D\'\iaz, B., Méndez-Padilla, J. A., & González-Aguilar, A. (2018). Primary tumors of the central nervous system. Clinical experience at a third level center. *Revista de Investigación Cl{\'\i}nica*, *70*(4), 177–183.

Hilton, D. A., & Hanemann, C. O. (2014). Schwannomas and their pathogenesis. *Brain Pathology*, *24*(3), 205–220.

Huang, G., Liu, Z., Van Der Maaten, L., & Weinberger, K. Q. (2017). Densely connected convolutional networks. *Proceedings of the IEEE Conference on Computer Vision and Pattern Recognition*, 4700–4708.

Joshi, A. A., & Aziz, R. M. (2024). Deep learning approach for brain tumor classification using metaheuristic optimization with gene expression data. *International Journal of Imaging Systems and Technology*, *34*(2), 1–16. https://doi.org/10.1002/ima.23007

Kaplan, K., Kaya, Y., Kuncan, M., & Ertunç, H. M. (2020). Brain tumor classification using modified local binary patterns (LBP) feature extraction methods. *Medical Hypotheses*, *139*(March). https://doi.org/10.1016/j.mehy.2020.109696

Katti, G., Ara, S. A., & Shireen, A. (2011). Magnetic resonance imaging (MRI)--A review. *International Journal of Dental Clinics*, *3*(1), 65–70.

Keras Applications. (n.d.). https://keras.io/api/applications

Komori, T. (2017). The 2016 WHO classification of tumours of the central nervous system: the major points of revision. *Neurologia Medico-Chirurgica*, *57*(7), 301–311.

Momin, A. A., Recinos, M. A., Cioffi, G., Patil, N., Soni, P., Almeida, J. P., Kruchko, C., Barnholtz-Sloan, J. S., Recinos, P. F., & Kshettry, V. R. (2021). Descriptive epidemiology of craniopharyngiomas in the United States. *Pituitary*, *24*, 517–522.

Neumann, H. P. H., Eggert, H. R., Weigel, K., Friedburg, H., Wiestler, O. D., & Schollmeyer, P. (1989). Hemangioblastomas of the central nervous system: a 10-year study with special reference to von Hippel-Lindau syndrome. *Journal of Neurosurgery*, *70*(1), 24–30.

Nibhoria, S., Tiwana, K. K., Phutela, R., Bajaj, A., & Chhabra, S. (2015). Histopathological spectrum of central nervous system tumors: A single centre study of 100 cases. *International Journal of Scientific Study*, *3*(6), 130–134.

Ostrom, Q. T., Gittleman, H., Fulop, J., Liu, M., Blanda, R., Kromer, C., Wolinsky, Y., Kruchko, C., & Barnholtz-Sloan, J. S. (2015). CBTRUS statistical report: primary brain and central nervous system tumors diagnosed in the United States in 2008-2012. *Neuro-Oncology*, *17*(suppl_4), iv1--iv62.

Pawełczyk, T., Pawełczyk, A., & Rabe-Jabłońska, J. (2012). Before you diagnose a patient with a conversion disorder, perform a thorough general medical and neurological examination. Case study. *Psychiatria Polska*, *46*(3), 483–492.

Phelps, M. E., & Mazziotta, J. C. (1985). Positron emission tomography: human brain function and biochemistry. *Science*, *228*(4701), 799–809.

Raschka, S. (2014). An overview of general performance metrics of binary classifier systems. *ArXiv Preprint ArXiv:1410.5330*.

Raza, A., Ayub, H., Khan, J. A., Ahmad, I., S. Salama, A., Daradkeh, Y. I., Javeed, D., Ur Rehman, A., & Hamam, H. (2022). A hybrid deep learning-based approach for brain tumor classification. *Electronics*, *11*(7), 1146.

Seetha, J., & Raja, S. S. (2018). Brain tumor classification using convolutional neural networks. *Biomedical \& Pharmacology Journal*, *11*(3), 1457.

Senan, E. M., Jadhav, M. E., Rassem, T. H., Aljaloud, A. S., Mohammed, B. A., Al-Mekhlafi, Z. G., & others. (2022). Early diagnosis of brain tumour mri images using hybrid techniques between deep and machine learning. *Computational and Mathematical Methods in Medicine*, *2022*.

Shankar, G. M., Balaj, L., Stott, S. L., Nahed, B., & Carter, B. S. (2017). Liquid biopsy for brain tumors. *Expert Review of Molecular Diagnostics*, *17*(10), 943–947.

Sheline, G. E. (1977). Radiation therapy of brain tumors. *Cancer*, *39*(S2), 873–881.

Siddiqui, M. F., Reza, A. W., & Kanesan, J. (2015). An automated and intelligent medical decision support system for brain MRI scans classification. *PloS One*, *10*(8), e0135875.

Szegedy, C., Vanhoucke, V., Ioffe, S., Shlens, J., & Wojna, Z. (2016). Rethinking the inception architecture for computer vision. *Proceedings of the IEEE Conference on Computer Vision and Pattern Recognition*, 2818–2826.

Tan, M., & Le, Q. (2019). Efficientnet: Rethinking model scaling for convolutional neural networks. *International Conference on Machine Learning*, 6105–6114.

Taylor, T., Dineen, R. A., Gardiner, D. C., Buss, C. H., Howatson, A., & Pace, N. L. (2014). Computed tomography (CT) angiography for confirmation of the clinical diagnosis of brain death. *Cochrane Database of Systematic Reviews*, *3*.

Thakor, N. V, & Tong, S. (2004). Advances in quantitative electroencephalogram analysis methods. *Annu. Rev. Biomed. Eng.*, *6*, 453–495.

Theodros, D., Patel, M., Ruzevick, J., Lim, M., & Bettegowda, C. (2015). Pituitary adenomas: historical perspective, surgical management and future directions. *CNS Oncology*, *4*(6), 411–429.